

# Two-Electron Redox Tuning of Cyclopentadienyl Cobalt Complexes Enabled by the Phenylenediamide Ligand

Minzhu Zou, Thomas J. Emge, Kate M. Waldie\*

Department of Chemistry and Chemical Biology, Rutgers, The State University of New Jersey,  
123 Bevier Road, Piscataway, New Jersey 08854, United States

[\\*kate.waldie@rutgers.edu](mailto:kate.waldie@rutgers.edu)

## ABSTRACT

A family of neutral cobalt complexes,  $[\text{Cp}^{\text{R}}\text{Co}(\text{Ropda})]$  **1-5**, based on the redox-active *o*-phenylenediamide ligand ( $\text{Ropda}$ ) undergo reversible  $2e^-$  oxidation revealed by cyclic voltammetry. This multielectron behavior is observed for all complexes regardless of the substituents on the phenylenediamide ligand, enabling redox tuning over more than 0.5 V. These diamagnetic neutral complexes are best described as delocalized systems with covalent bonding across the cobalt-opda metallocycle, consistent with the closed-shell singlet ground-state predicted by density functional theory (DFT) calculations. Two-electron oxidation using chemical oxidants affords the dicationic species, which are formulated as Co(III)-benzoquinonediimine systems with an additional coordinated acetonitrile ligand. DFT calculations also predict an *ECE* pathway for the  $2e^-$  oxidation, in which the first  $1e^-$  step is primarily a ligand-based process with redistribution of electron density to the metal. The associated distortion of the coordination geometry and disruption of the metallocycle bonding enable acetonitrile coordination in the intermediate oxidation state, which is critical for favoring the second electron transfer and accessing the potential inversion.

## INTRODUCTION

The transfer of multiple electrons through redox processes is central to many chemical, electrochemical, and biological transformations. While prevalent at late second- and third-row transition metal complexes based on noble metal centers,  $2e^-$  redox couples are rare at mononuclear first-row transition metal systems, which instead favor sequential  $1e^-$  transfer events

at well-separated potentials due to the high electrostatic penalty associated with the second transfer. This behavior often poses a fundamental challenge, resulting in  $1e^-$  radical-based reactivity or larger overpotentials for electrocatalytic reactions with the more earth-abundant 3d metals.<sup>1</sup> An overall  $2e^-$  redox process can be accomplished when the second electron transfer is more energetically favorable than the first, a situation known as potential inversion.<sup>2</sup> Structural reorganization, solvation effects, or ion-pairing may play a large role in accessing this behavior.<sup>3</sup> <sup>4</sup> Developing first-row transition metal complexes that can mediate multielectron processes and thus mimic noble metal reactivity continues to be of great interest.<sup>5-9</sup>

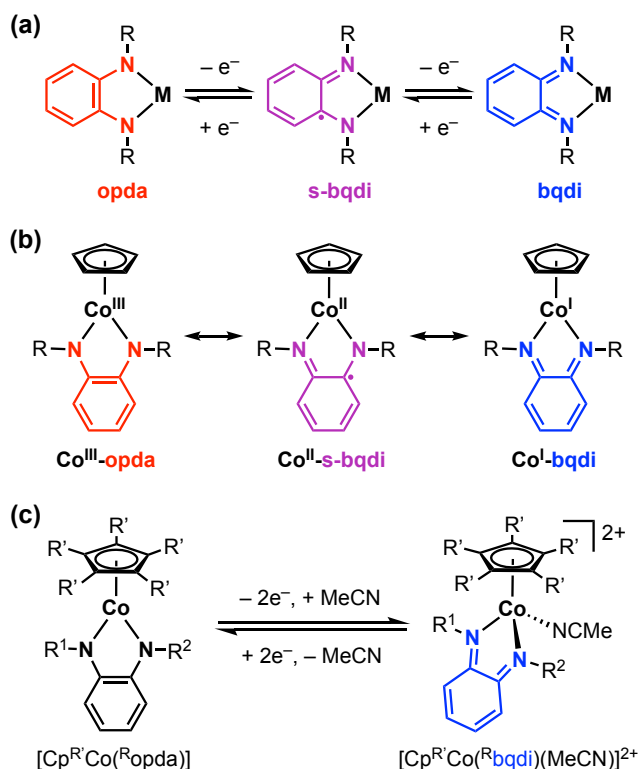
Redox-active ligands have emerged as another strategy for accessing greater redox flexibility and multielectron behavior at first-row metal complexes due to their ability to serve as electron reservoirs.<sup>10-14</sup> The design of many redox-active ligands is inspired by metalloenzymes, which often facilitate multielectron transformations through the combination of transition metal cations and redox cofactors. One of the best known examples is galactose oxidase, where cooperation between  $Cu^{II}$  and a tyrosyl-radical ligand enables the  $2e^-$  oxidation of alcohols.<sup>15</sup> However, introduction of a redox-active ligand into a transition metal complex does not guarantee that  $2e^-$  processes will be favored over  $1e^-$  reactivity. In fact, only a handful of mononuclear first-row metal complexes with redox-active ligands exhibit a  $2e^-$  redox couple, often accompanied by ligand coordination or dissociation that promotes potential inversion.<sup>16-26</sup> Among these reports,  $2e^-$  reductions are more common; to our knowledge, only one reported system has shown a reversible  $2e^-$  oxidation.<sup>18</sup>

A classic redox-active ligand is *o*-phenylenediamide (opda), which has three readily accessible oxidation states when bound to a metal center: the dianionic opda, the monoanionic semibenzoquinonediimine (s-bqdi), and the neutral benzoquinonediimine (bqdi) (Scheme 1a). For opda and analogous catechol (*O,O*) and amidophenolate (*N,O*), the ligand oxidation states are accessed via sequential one-electron transfers.<sup>27-28</sup> Due to the possible non-innocence of these ligands, investigations into the electronic structure and reactivity of numerous transition metal complexes have been the subject of significant research efforts.<sup>18,28-36</sup> In a remarkable example, a  $Co^{III}$ -bis(amidophenolate) complex undergoes oxidative addition of alkyl halides, where each redox-active ligand supplies one electron to form the new  $Co^{III}$ -R bond.<sup>37</sup> A related  $Co^{II}$ -(s-bqdi)<sub>2</sub> complex catalyzes the reductive homocoupling of benzyl bromide, mediated by ligand-centered electron transfer.<sup>38</sup> Despite these transformations being overall  $2e^-$  processes, both cobalt

complexes exhibit discrete  $1e^-$  redox events, thus requiring greater overpotential to access this reactivity.

The half-sandwich complex  $[\text{CpCo}^{\text{I}}\text{opda}]$  (**1**; Cp = cyclopentadienyl) was first reported in 1967.<sup>39</sup> The electronic structure of this family of complexes may fall under one of three limiting descriptions with localized bonding (Scheme 1b). For a mono-substituted opda example, Trogler and co-workers proposed a delocalized  $\pi$ -bonding classification across the five-membered ring metallocycle,<sup>40</sup> while other authors have preferred the Co(I)-bqdi description for **1** and closely related  $[\text{CpCo}]$  or  $[\text{Cp}^*\text{Co}]$  systems (Cp\* = pentamethylcyclopentadienyl).<sup>41-45</sup> Additionally, recent electrochemical studies showed that **1** and a perfluoro analogue can be reversibly oxidized at mild potentials, though minimal discussion on the nature of this redox process was provided and it appears to be assigned as a  $1e^-$  wave despite the peak current being significant greater than expected for single electron transfer.<sup>44-45</sup> Thus, further investigations are needed to clarify the electronic structure and electrochemical behavior of these cobalt complexes.

**Scheme 1.** (a) Ligand oxidation states for general metal-phenylenediamide complexes. (b) Possible electronic structure representations of  $[\text{CpCo}^{\text{R}}\text{opda}]$  complexes. (c) Reversible  $2e^-$  oxidation of  $[\text{Cp}^{\text{R}}\text{Co}^{\text{R}}\text{opda}]$  complexes.

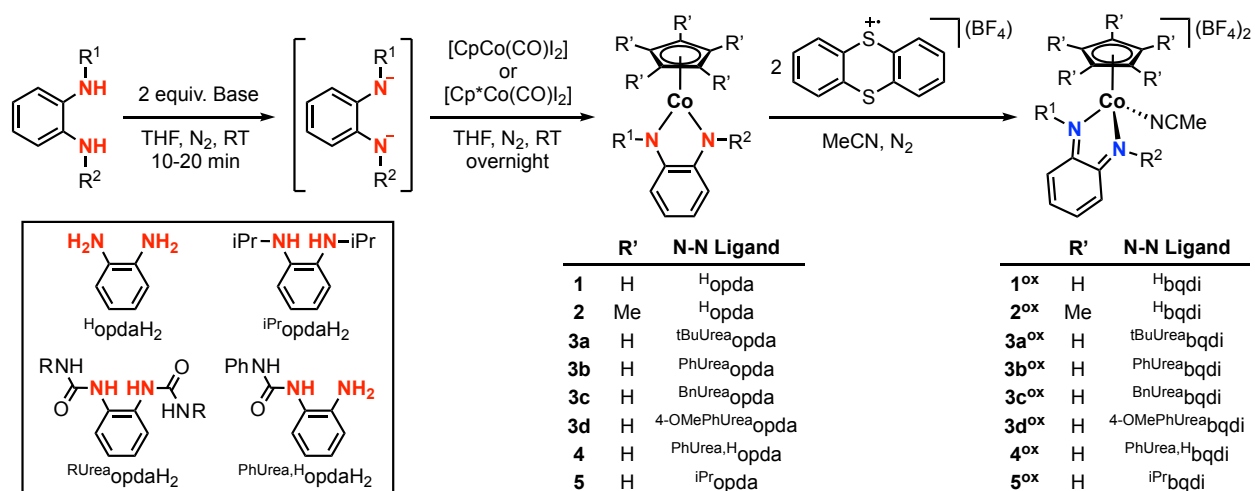


Herein, we describe a series of neutral half-sandwich cobalt complexes bearing the  ${}^R\text{opda}$  ligand. We unambiguously demonstrate that these complexes undergo reversible  $2e^-$  oxidation, affording a significant new example of potential inversion and multielectron activity, in particular multielectron oxidation, at first-row transition metal complexes. This redox behavior is maintained for all complexes in this series, with the  $2e^-$  oxidation potential shifting by more than 0.5 V depending on the ligand electronic properties. Independent synthesis and characterization of the doubly-oxidized dicationic complexes confirm that  $2e^-$  oxidation generates a  $\text{Co}^{\text{III}}$  center with a neutral bqdi ligand (Scheme 1c). Experimental and computational analyses indicate covalent  $\pi$ -bonding interactions between the cobalt and redox-active ligand in the neutral complexes and shed further light on the sites of electron transfer. The structural and geometry changes that accompany  $2e^-$  oxidation point to the active involvement of the redox-active ligand in this process.

## RESULTS

**Synthesis.** In general, the substituted phenylenediamine ligands ( ${}^R\text{opdaH}_2$ ) were prepared by reaction of *o*-phenylenediamine with the appropriate isocyanate (for  $R = \text{ureayl}$ ) or 2-iodopropane (for  $R = \text{isopropyl}$ ), following previously reported or modified procedures.<sup>46-48</sup> The synthesis of the neutral cobalt complexes **1-5** was performed by initial deprotonation of  ${}^R\text{opdaH}_2$  with 2 equiv. base in anhydrous THF, followed by salt metathesis with  $\text{CpCo}(\text{CO})\text{I}_2$  or  $\text{Cp}^*\text{Co}(\text{CO})\text{I}_2$  (Scheme 2). Alternate syntheses of **1** and **2** have also been reported using aqueous sodium hydroxide.<sup>49-50</sup> All neutral complexes were isolated as crystalline solids with very intense dark color.

**Scheme 2.** Synthetic procedures for preparing neutral and dicationic cobalt complexes.



These neutral cobalt complexes are diamagnetic and display well-resolved, sharp signals by  $^1\text{H}$  NMR, in agreement with previous reports on **1** and **2**.<sup>49-50</sup> Variable temperature NMR spectra for **3a** show no signal broadening or chemical shift changes (except the NH signal) up to 45 °C (Figure S24), and magnetic susceptibility measurements using Evans method are consistent with a singlet ground state. The Cp signal for **3-5** appears in the range of 4.9-5.2 ppm, similar to that of **1** at 5.01 ppm. The isopropyl C–H in **5** is a broad signal at 25 °C, which is attributed to rotation of the isopropyl groups in solution. Different conformations of **5** with respect to the isopropyl group orientations become distinguishable at lower temperatures (Figure S37).

Treatment of the neutral complexes with 2 equiv. chemical oxidant yields the doubly-oxidized, dicationic complex  $[\text{Cp}^{\text{R}'}\text{Co}(\text{R}^{\text{bqdi}})(\text{MeCN})]\text{X}_2$  ( $\text{R}' = \text{H}$  or  $\text{CH}_3$ ,  $\text{X} = \text{PF}_6^-$  or  $\text{BF}_4^-$ ) in 89-96% isolated yield (Scheme 2). In general, while silver hexafluorophosphate ( $\text{AgPF}_6$ ) may be used as the chemical oxidant, we found that thianthrenium tetrafluoroborate ( $(\text{Thi}^{++})\text{BF}_4$ ,  $E_{1/2} = 0.86$  V vs.  $[\text{Cp}_2\text{Fe}]^{+/0}$ )<sup>51</sup> resulted in cleaner reactivity with less decomposition. For example, layering of **1** with 2 equiv.  $\text{AgPF}_6$  in  $\text{MeCN}/\text{Et}_2\text{O}$  at –35 °C yields  $[\text{CpCo}(\text{H}^{\text{opdaH}_2})(\text{MeCN})][\text{PF}_6]_2$  (**[1-H<sub>2</sub>][PF<sub>6</sub>]<sub>2</sub>**) as red crystals, confirmed through independent synthesis of this complex (see Supporting Information). However, following the same oxidation procedure using  $(\text{Thi}^{++})\text{BF}_4$  generates **1<sup>ox</sup>** with only minor amounts of **[1-H<sub>2</sub>][BF<sub>4</sub>]<sub>2</sub>** (Figure S38). Chemical oxidation to generate **2<sup>ox</sup>** and **5<sup>ox</sup>** can be performed under ambient conditions, while **1<sup>ox</sup>**, **3a<sup>ox</sup>-3d<sup>ox</sup>**, and **4<sup>ox</sup>** require low temperature synthesis.

By  $^1\text{H}$  NMR, the  $2e^-$  oxidation of **3-5** is accompanied by a downfield shift of the Cp peak from ca. 5.0 ppm to ca. 6.3 ppm. This chemical shift is comparable to that of other low-spin, dicationic  $\text{Co}^{\text{III}}$  half-sandwich complexes.<sup>52-54</sup> Surprisingly, the Cp\* peak in **2** is shifted slightly upfield upon oxidation. The  $^1\text{H}$  NMR spectrum of **2<sup>ox</sup>** also shows a singlet at 11.80 ppm for the ligand NH protons (Figure S42), consistent with a “C=NH” imine-type group in a bqdi ligand.<sup>55</sup> Given that the chemical shift of the NH signal in **2** is significantly more upfield (8.37 ppm), it appears reasonable to discount the  $\text{Co}^{\text{I}}$ -bqdi description of the neutral complexes (Scheme 1b).

The  $^1\text{H}$  NMR analysis also reveals that the solution-phase stability of the oxidized complexes depends on the ligand. Complexes **3a<sup>ox</sup>-3d<sup>ox</sup>** and **4<sup>ox</sup>** are stable in  $\text{CD}_3\text{CN}$  at –20 °C, but slowly decompose to  $[\text{CpCo}(\text{MeCN})_3]^{2+}$  and unidentified species over 16 hours at 0 °C (Figure S47). Solutions of **1<sup>ox</sup>** and **2<sup>ox</sup>** in  $\text{CD}_3\text{CN}$  are stable for at least 5 hours at 4 °C (Figures S39 and S44). We anticipated that the alkyl groups in **5** would improve the stability of the oxidized complex, and

indeed, **5<sup>ox</sup>** shows much better thermal and air-stability. No changes are observed by <sup>1</sup>H NMR when a solution of **5<sup>ox</sup>** in CD<sub>3</sub>CN is exposed to air for 28 h under ambient conditions (Figure S61).

**X-Ray Crystallography.** Single crystals of the neutral complexes and <sup>t</sup>BuUrea<sub>opda</sub>H<sub>2</sub> suitable for X-ray diffraction were obtained from slow evaporation of a dilute Et<sub>2</sub>O/hexanes solution (for **3a** and **5**), slow evaporation of a saturated MeCN solution (for **3b-3d** and **4**), or vapor diffusion of hexanes into a THF solution (for <sup>t</sup>BuUrea<sub>opda</sub>H<sub>2</sub>) at room temperature. The crystal structure of **5** is shown in Figure 1a; structures of the other neutral complexes are presented in the Supporting Information. These complexes show a T-shaped, two-legged piano stool geometry, where the Cp ligand plane is nearly perpendicular to the Co-phenylenediamide plane. The phenylene backbone shows a small degree of alternation in the C–C bond lengths between 1.40-1.43 Å and 1.35-1.38 Å, indicating some loss of aromaticity compared to free *o*-phenylenediamine. These results are consistent with the structures of **1** and **2**, which have been previously reported.<sup>42-43</sup>

For the ureayl systems **3a-3d** and **4**, two cobalt complexes are associated in the unit cell with intermolecular hydrogen bonding between the ureayl carbonyl and NH groups. The average Co–N and N–C<sub>phenylene</sub> bond lengths for **3a-3d** are 1.86 ± 0.01 Å and 1.37 ± 0.01 Å, respectively, which are shorter than typical Co–N and N–C single bonds and suggest the presence of  $\pi$ -conjugation across the Co-opda metallocycle.<sup>18,31-32</sup> In contrast, the N–C<sub>phenylene</sub> bond lengths in <sup>t</sup>BuUrea<sub>opda</sub>H<sub>2</sub> are 1.442(11) Å, ca. 0.07 Å longer than the corresponding bonds in **3a**. Complex **4**, which only has one ureayl arm, shows two distinct Co–N bond distances: on the ureayl side, the Co–N bond length (1.870(3) Å) is similar to **3a**, while the Co–N bond length is much shorter (1.834(3) Å) on the unsubstituted NH side. In fact, the latter is comparable to the Co–N bond length in **1**.<sup>42</sup>

The crystal structure of **5** is similar to the other neutral complexes; however, as shown in Figure 1a, the two isopropyl groups exhibit different orientations in the crystal lattice. One isopropyl methine C–H is directed toward the Cp ligand, while the other methine C–H is directed toward the phenylene backbone, resulting in a short intramolecular nonbonded H...H contact (1.84 Å). In this complex, steric repulsion can exist between the isopropyl CH<sub>3</sub> groups and the hydrogens on the Cp ligand or phenylene ring. While the *trans* orientation was found in this crystal structure, both the *trans* and *syn* geometries are accessible in solution by rotation of the isopropyl C–N bond, as observed by <sup>1</sup>H NMR (*vide supra*).

While we could not obtain crystals of **3a<sup>ox</sup>**-**3d<sup>ox</sup>** and **4<sup>ox</sup>** due to facile ligand loss and formation of  $[\text{CpCo}(\text{MeCN})_3]^{2+}$ , red single crystals of **2<sup>ox</sup>** and **5<sup>ox</sup>** were grown by vapor diffusion from MeCN/Et<sub>2</sub>O at -35 °C, and red needles of **1<sup>ox</sup>** were obtained via slow diffusion of an Et<sub>2</sub>O solution of **1** into an MeCN solution of (Thi<sup>+</sup>)BF<sub>4</sub> at -35 °C. Selected bond lengths of **5** and **5<sup>ox</sup>** are given in Figure 1; structural metrics of the other oxidized complexes are provided in the Supporting Information. Compared to their neutral analogues, the dicationic complexes have a higher coordination number with a bound acetonitrile ligand. While the distance between the cobalt center and the cyclopentadienyl plane (Cp or Cp\*) is not significantly affected by oxidation (Tables S27-S29), there is clear elongation of the Co–N bond lengths (0.1 Å longer). The N–C<sub>phenylene</sub> bond lengths in the oxidized complexes are shorter (by 0.03-0.06 Å), consistent with typical C=N double bonds. Also, the phenylene backbone shows alternating C–C bond distances between single bonds (ca. 1.44 Å) and double bonds (ca. 1.34 Å).

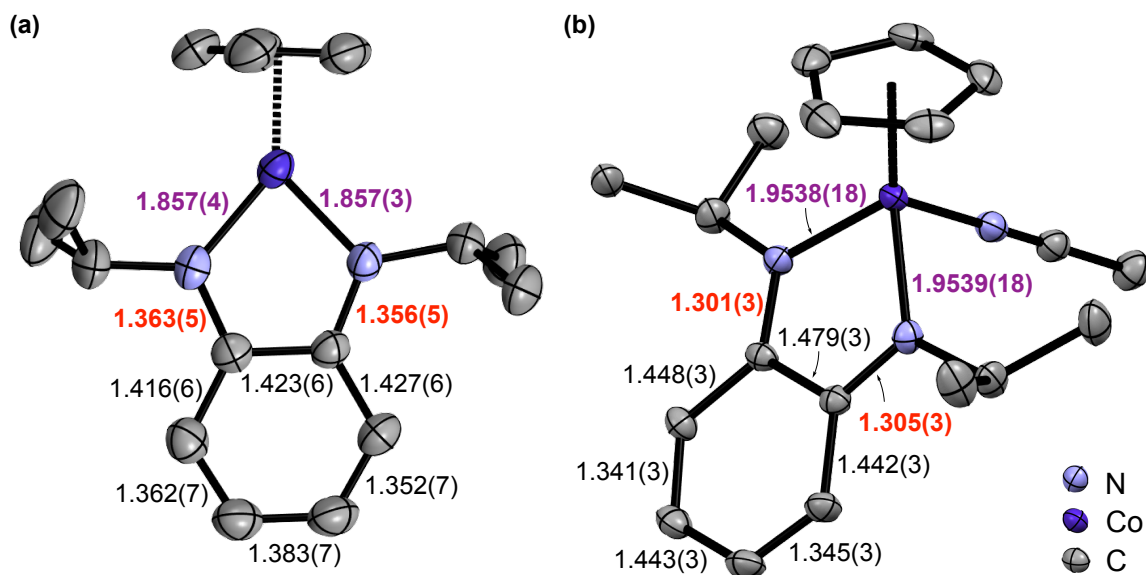


**Figure 1.** Structure of (a) **5**, and (b) **5<sup>ox</sup>** with selected bond lengths (Å). Hydrogen atoms, co-crystallized solvent, and BF<sub>4</sub><sup>-</sup> counterions omitted for clarity. Ellipsoids shown at 50% probability.

**Electrochemistry.** Cyclic voltammetry (CV) studies of **1-5** display one reversible oxidation and one reversible reduction in 0.1 M [*n*Bu<sub>4</sub>N][PF<sub>6</sub>] in MeCN (Figure 2). Key details for these redox couples are summarized in Table 1. Notably, the peak-to-peak separation ( $\Delta E_p$ ) at 25 mV/s for the oxidation of **1** and **2** is only 46 and 31 mV, respectively, while  $\Delta E_p$  is 75 mV for the

reduction of **1** at the same scan rate (Figures S64 and S65). The oxidation peak current is 2.4-2.7 times higher than that of the reduction for all complexes. These observations are consistent with a  $2e^-$  oxidation and  $1e^-$  reduction.<sup>56</sup> The reversibility of the  $2e^-$  wave is maintained over a range of scan rates, and no evidence of discrete  $1e^-$  events is observed (see Supporting Information). This behavior is indicative of potential inversion, where the second electron loss occurs at a more negative potential. Consistent with this assignment, **5<sup>ox</sup>** shows a  $2e^-$  reduction at the same potential as the  $2e^-$  oxidation of **5** (Figures S85 and S86). The  $2e^-$  redox couple of these complexes is in stark contrast to the electrochemistry of related square planar or tetrahedral cobalt complexes with opda-type ligands, which exhibit separate  $1e^-$  processes.<sup>18,26,32,38,57</sup> This novel but previously overlooked multielectron behavior motivated our further investigation into these complexes.

**Table 1.** Cyclic Voltammetry Data of Complexes **1-5** and **5<sup>ox</sup>**.<sup>a</sup>

Complex	$E_{1/2}^b$ (V)	$\Delta E_p^c$ (mV)	$i_c/i_a^d$	$E_{1/2}^b$ (V)	$\Delta E_p^c$ (mV)	$i_c/i_a^d$
<b>1</b>	-0.11	62	0.96	-1.83	75	1.07
<b>2</b>	-0.33	69	0.93	-2.04	81	1.05
<b>3a</b>	0.11	75	1.03	-1.24	74	1.00
<b>3b</b> <sup>e</sup>	0.20	80	0.89	-1.03	77	1.08
<b>3c</b> <sup>e</sup>	0.15	59	0.94	-1.18	69	1.14
<b>3d</b> <sup>e</sup>	0.18	61	0.86	-1.07	67	1.06
<b>4</b>	0.045	69	0.94	-1.35	72	1.10
<b>5</b>	-0.17	75	0.97	-1.87	77	1.24
<b>5<sup>ox</sup></b> <sup>f</sup>	-0.17	55	1.08	-1.88	80	1.21

<sup>a</sup>Conditions: 1 mM [Co] in 0.1 M [<sup>n</sup>Bu<sub>4</sub>N][PF<sub>6</sub>] in MeCN, glassy carbon working electrode, Pt counter electrode, Ag/AgNO<sub>3</sub> reference electrode, measured at 100 mV/s. <sup>b</sup> $E_{1/2} = (E_{p,a} + E_{p,c})/2$ , where  $E_{p,a}$  and  $E_{p,c}$  are anodic and cathodic peak potentials, respectively. Potentials versus [Cp<sub>2</sub>Fe]<sup>+0</sup>. <sup>c</sup> $\Delta E_p = E_{p,a} - E_{p,c}$ . <sup>d</sup> $i_{p,a}$  = anodic peak current,  $i_{p,c}$  = cathodic peak current. <sup>e</sup>Solvent = MeCN/THF (4:1). <sup>f</sup>0.5 mM [Co].

Complexes **3a-3d** and **4** with electron-withdrawing ureayl groups exhibit the most positive redox potentials in this series, with the potential of the  $1e^-$  feature being influenced more

significantly. Varying the substituents on the ureayl arms has limited effect on the  $2e^-$  oxidation, but changing the number of ureayl groups shifts the oxidation by ca. 150 mV per substituent (comparing **1**, **3b**, and **4**; see Table 1). The introduction of electron-donating isopropyl groups in **5** shifts both redox couples more negative due to increased electron density at the metal and redox-active ligand. The electron-rich Cp\* ligand in **2** has an even more significant impact on redox potentials, which are both shifted negative by ca. 200 mV compared to **1**, the Cp analogue. It is well-known that the redox potentials of metal complexes shift depending on the electron-donating or withdrawing nature of the ligands. However, this series is a remarkable demonstration where the oxidation potential can be tuned by more than 0.5 V while maintaining reversible  $2e^-$  behavior.

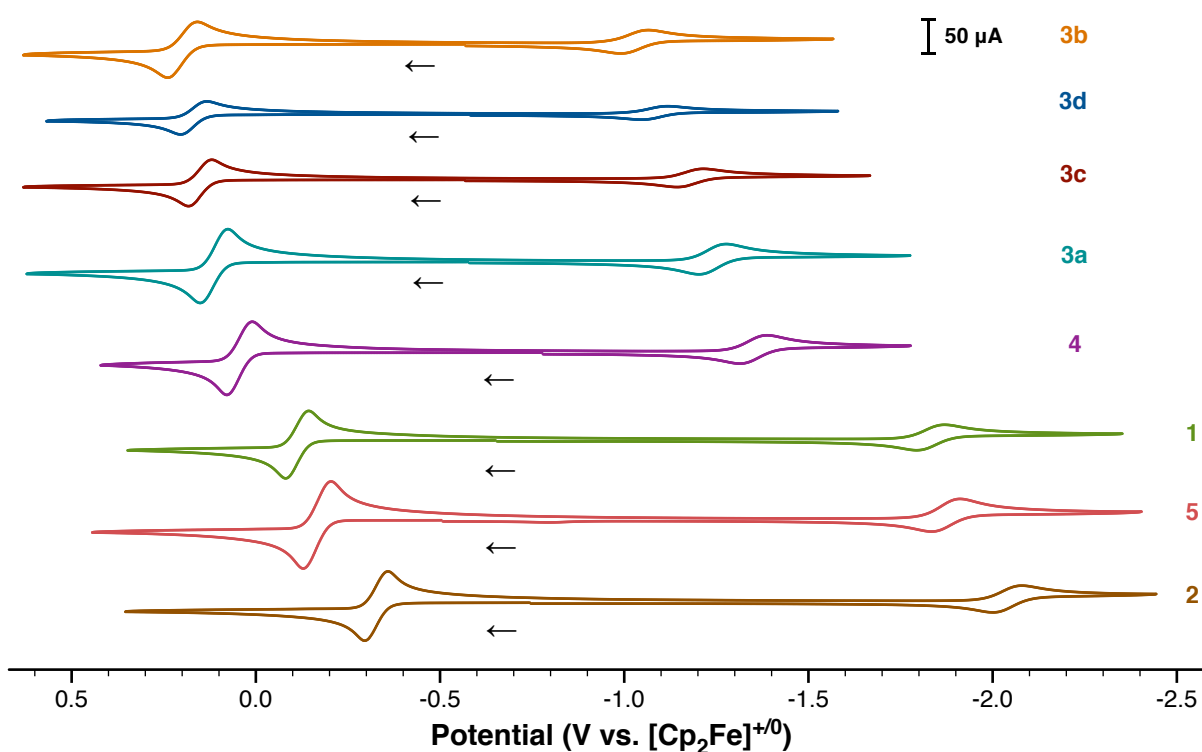


**Figure 2.** Cyclic voltammograms of cobalt complexes in MeCN (**1**, **2**, **3a**, **4**, and **5**) or MeCN/THF (4:1; **3b**, **3c**, and **3d**) (1 mM [Co] and 0.1 M [ $n$ Bu<sub>4</sub>N][PF<sub>6</sub>]; scan rate 100 mV/s).

The  $2e^-$  oxidation remains reversible in CH<sub>2</sub>Cl<sub>2</sub> or THF with 0.2 M [ $n$ Bu<sub>4</sub>N][PF<sub>6</sub>] (see Supporting Information), demonstrating that the potential inversion is still favorable with weakly coordinating solvents and/or supporting electrolyte ions. The oxidation of **3b** in MeCN with 0.05 M [ $n$ Bu<sub>4</sub>N][BARF<sub>24</sub>] (BARF<sub>24</sub><sup>-</sup> = tetrakis[3,5-bis(trifluoromethyl)phenyl]borate) shows partial loss

of reversibility at slow scan rates ( $i_{p,c}/i_{p,a} = 0.60$  at 100 mV/s), but gradual addition of [<sup>n</sup>Bu<sub>4</sub>N][PF<sub>6</sub>] increases reversibility (Table S20 and Figure S80). Surprisingly, the oxidation of **2** is reversible in 0.05 M [<sup>n</sup>Bu<sub>4</sub>N][BArF<sub>24</sub>] in MeCN or at faster scan rates in CH<sub>2</sub>Cl<sub>2</sub> (Figures S71 and S72), and thus the reversibility of this feature appears to depend on the ligand identity and solution conditions. The large, non-coordinating BArF<sub>24</sub><sup>-</sup> anion may be unable to provide sufficient stabilization to the sterically bulky oxidized complexes such as **3b<sup>ox</sup>**.

**Electronic Absorption Spectroscopy.** The electronic absorption spectra of the neutral cobalt complexes are provided in the Supporting Information (Figures S87-S95); the spectrum of **5** in MeCN is highlighted in Figure 3a (orange trace). In line with the intense colors of these complexes, the electronic spectra show a dominant transition in the visible region at ca. 520-580 nm with molar absorption coefficients on the order of 20,000 M<sup>-1</sup>·cm<sup>-1</sup> (Table 2). The presence of ureayl substituents causes a red-shift of this absorbance for **3a-3d** and **4** compared to **1**. A weak absorption is also observed in the NIR region between 700-800 nm.

**Table 2.** Electronic Spectral Data for Complexes **1-5**.

Complex	$\lambda_{\max}$ (nm)	$\epsilon$ (M <sup>-1</sup> ·cm <sup>-1</sup> )
<b>1</b>	525	21,100
<b>2</b>	577	24,500
<b>3a</b>	565	17,800
<b>3b</b>	583	17,800
<b>3c</b>	573	17,900
<b>3d</b>	582	16,300
<b>4</b>	556	17,900
<b>5</b>	524	16,600

Time-dependent DFT (TD-DFT) calculations and natural transition orbital (NTO) analysis were used to clarify the main molecular orbital contributions to these electronic transitions (see Supporting Information for details). The calculated transitions for **5** (Figures 3c) and the other neutral complexes (Figures S112-S114) provide a reasonable match with the main features of the experimental spectrum for each system. The intense visible absorption is mainly attributed to the

HOMO-1  $\rightarrow$  LUMO transition, which has significant  $\pi \rightarrow \pi^*$  character across the Co–N bonds (Figure 3d). The weak NIR absorption corresponds to the approximate HOMO  $\rightarrow$  LUMO transition, where the HOMO has cobalt  $d_{xy}$  and phenylenediamide  $\pi$  characters. Similar assignments are obtained for the other neutral complexes (Tables S34-S36).

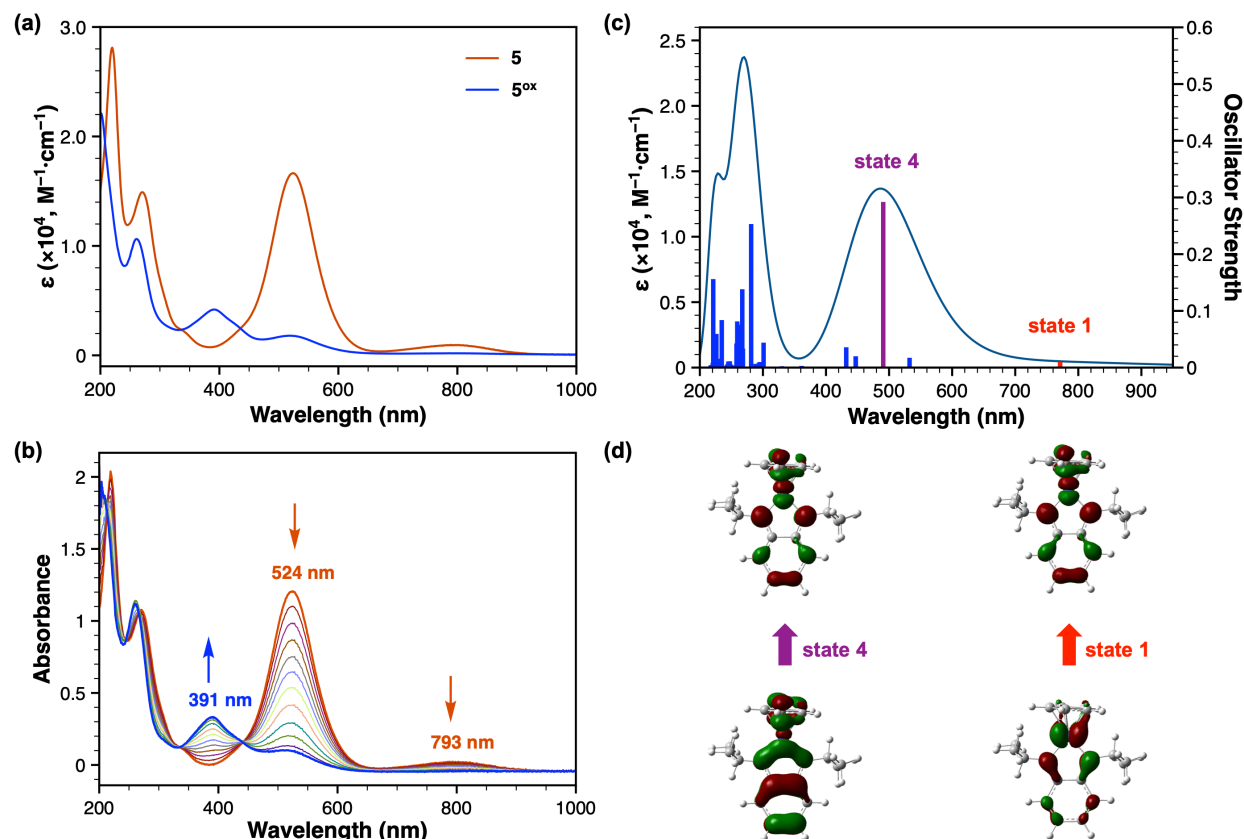


**Figure 3.** (a) Electronic absorption spectrum of **5** and **5<sup>ox</sup>** in MeCN. (b) UV-vis-SEC oxidation of **5** in MeCN. See Supporting Information for experimental details. (c) Calculated electronic spectrum of **5** based on the TD-DFT wavelengths and oscillator strengths using Gaussian functions of hwhm = 2686  $\text{cm}^{-1}$ . (d) Representative natural transition orbitals of **5** for selected electronic transitions. See Supporting Information for computational details.

Upon oxidation, the absorption profile of **5<sup>ox</sup>** in the visible region is significantly decreased with weak transitions at 518 nm ( $\epsilon = 1,800 \text{ M}^{-1}\cdot\text{cm}^{-1}$ ) and 391 nm ( $\epsilon = 4,200 \text{ M}^{-1}\cdot\text{cm}^{-1}$ ), along with a shoulder around 425 nm (Figure 3a, blue trace). Complex **5<sup>ox</sup>** shows good stability in solution for at least 28 hours under ambient conditions. Given the limited solution stability of the other oxidized

complexes, electronic absorption studies of independently isolated samples were unreliable. However, we found these species to be stable on the spectroelectrochemistry (SEC) timescale, and thus UV-Vis-SEC studies were employed to probe changes in the electronic absorption profile *in situ* upon  $2e^-$  oxidation. As shown in Figure 3b, monitoring the oxidation of **5** shows a decrease of the characteristic bands at 524 and 793 nm, with the simultaneous appearance of new band at 391 nm, consistent with the absorption profile of independently prepared **5<sup>ox</sup>**. Isosbestic points appear at 335 and 442 nm. No evidence of an intermediate oxidation state was observed. UV-Vis-SEC studies of **1**, **2**, **3a**, and **4** show similar behavior as the electrode potential is scanned more positive (Figures S97-100), with disappearance of the strong visible transition and appearance of a new band at 380-420 nm for the oxidized species.

**Computation Studies.** Density-functional theory (DFT) calculations were performed to gain a better understanding of the electronic structure of these complexes and the origins of the  $2e^-$  oxidation. Complex **3a** was selected for the initial evaluation of different functionals since the bulky ureayl groups may affect the optimized geometry.<sup>58</sup> Ground-state geometry optimizations of **3a** as a closed-shell singlet using pure or hybrid functionals were able to reproduce the T-shaped geometry and key structural metrics with negligible differences (within 0.04 Å and 1.1°, respectively) between the DFT-calculated and X-ray structures (Tables S25 and S26). From comparing the calculated results with the full set of spectroscopic and electrochemical data for **3a**, we find that the BP86 and PBE functionals with TZVPP (for Co) and TZVP (for other atoms) basis set show reliable results. Since the BP86 functional has shown success for predicting the structural and redox properties of late-transition metal complexes,<sup>59</sup> this functional was selected for further computational analysis of this family of complexes.

Additionally, we considered the antiferromagnetically coupled singlet biradical as a possible electronic description of **3a**, which would also be consistent with the diamagnetic nature of the neutral complexes. Accessing the antiferromagnetically coupled  $\text{Co}^{\text{II}}(\text{low-spin})\text{-(s-bqdi)}$  using the broken-symmetry (BS) approach failed with BP86 and other pure functionals, instead optimizing to a closed-shell singlet with no unpaired spin density. Similar observations have been reported for BS calculations with square planar nickel complexes bearing two s-bqdi ligands, which may be attributed to the overestimation of the stability of spin-paired states by pure functionals.<sup>60</sup> On the other hand, the BS state of **3a** using hybrid functionals was successfully computed, having

unpaired spin density located on both the cobalt and the phenylenediamide ligand (Figure S103). The antiferromagnetically coupled biradical is slightly lower in energy (-1.38 kcal/mol) than the spin-paired singlet; however, the optimized geometry shows larger deviations from the crystal structure. More significantly, the singlet biradical is not predicted to undergo a  $2e^-$  oxidation, which contradicts our experimental data (Table S32). Thus, the closed shell singlet is taken as the most reasonable electronic structure description for the neutral cobalt complexes.

Using our selected computational approach, we observe close agreement between the X-ray structure and calculated geometry for all neutral cobalt complexes and the isolated oxidized species (Tables S27-S29). Importantly, the increase in the Co–N bond lengths and decrease in the N–C<sub>phenylene</sub> bond lengths upon  $2e^-$  oxidation are effectively reproduced in the calculated structures, as is the loss of aromaticity in the phenylene ring. Additionally, our DFT calculations predict that the *trans* geometry of **5** is slightly lower in energy (ca. 1 kcal/mol) compared to the two possible *syn* geometries (Figure S102). The energetic accessibility of these conformations is consistent with the fluxional behavior of the isopropyl groups in **5** observed by  $^1\text{H NMR}$  (*vide supra*).

The calculated potential for the first  $1e^-$  oxidation of **3a** is  $E_{\text{ox}1} = 0.15$  V vs.  $[\text{Cp}_2\text{Fe}]^{+/0}$ , which is in excellent agreement with the experimental value for the  $2e^-$  CV feature ( $E_{1/2} = 0.11$  V vs.  $[\text{Cp}_2\text{Fe}]^{+/0}$ ). The calculated  $E_{\text{ox}1}$  values for the other neutral complexes also show good agreement with the CV data and largely reproduce the observed trends as a function of ligand substituents (Table S32). With each system, loss of one electron results in a monocationic complex in which the calculated spin density is mainly centered on cobalt (low-spin,  $S_{\text{total}} = 1/2$ , Figure 4a and Figures S104-S106), though we note  $[\mathbf{2}]^+$  also has appreciable spin density on the ligand. The  $1e^-$  oxidation is accompanied by elongation of the Co–N bond lengths and shortening of the N–C<sub>phenylene</sub> bond lengths, along with systematic changes to the phenylene backbone (Tables S30 and S31). There is also a noticeable change in the dihedral angle between the cyclopentadienyl and the N–Co–N planes ( $9\sim 13^\circ$ ).

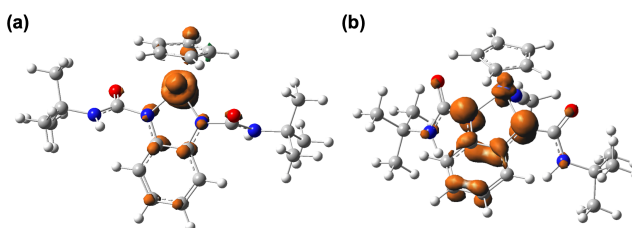
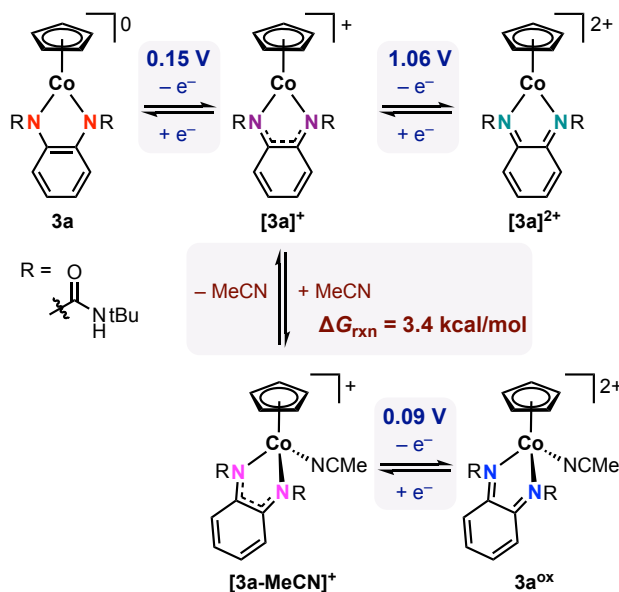


**Figure 4.** Spin density plots of the monocationic complexes (a)  $[\mathbf{3a}]^+$ , and (b)  $[\mathbf{3a-MeCN}]^+$ .

Following  $1e^-$  oxidation, coordination of acetonitrile is slightly uphill (Table S33). From here, the calculated potential for the second electron loss is in excellent agreement with the experimentally observed  $2e^-$  feature. For example, the calculated oxidation potential for  $[\mathbf{3a-MeCN}]^+$  is  $E_{ox2} = 0.09$  V vs.  $[\text{Cp}_2\text{Fe}]^{+/0}$ , 60 mV more negative than the predicted oxidation of  $\mathbf{3a}$ . Thus, the oxidation pathway for these complexes is best described by an *ECE* mechanism. Indeed, potential inversion by this route is predicted for all complexes except for  $\mathbf{3b}$  (where the difference between  $E_{ox1}$  and  $E_{ox2}$  is only 5 mV, see Table S32). The possibility of an *EEC* mechanism was also considered, where two  $1e^-$  transfer events are followed by acetonitrile coordination. However, in the absence of MeCN coordination, the second  $1e^-$  oxidation is ca. 21 kcal/mol more uphill compared to the first oxidation (Scheme 3).

**Scheme 3.** Calculated square scheme for oxidative electron transfer and acetonitrile coordination. Values are shown for  $\mathbf{3a}$ . Potentials are given in V vs.  $[\text{Cp}_2\text{Fe}]^{+/0}$ .  $\Delta G_{rxn}$  is given in kcal/mol.



Interestingly, coordination of the acetonitrile ligand to  $[\mathbf{3a}]^+$  causes the unpaired spin density to shift significantly from cobalt to the ligand backbone in  $[\mathbf{3a-MeCN}]^+$  (Figure 4b). At the same time, the predicted Co–N bond lengths increase from ca. 1.89 Å to 1.94 Å and the predicted N–C<sub>phenylene</sub> bond lengths increase from 1.34 Å to 1.36 Å, with small changes to the phenylene backbone bond lengths as well (Table S30). Notably, the nature of these changes depends on the ligand substituents. Focusing on the  $[\text{CpCo}]$  systems, the calculated spin density for  $[\mathbf{1-MeCN}]^+$

is located on the metal with some spin density on the ligand, while the more electron-rich isopropyl complex **[5-MeCN]<sup>+</sup>** is predicted to have the spin density more centered on cobalt (Figures S104 and S106). This behavior is mirrored in the predicted bond length changes, where only slight differences in bond metrics are seen upon MeCN coordination to **[1]<sup>+</sup>** and **[5]<sup>+</sup>** (see Table S31).

The frontier molecular orbitals in this series also show differing behavior based on the ligand identity (Figure 5). The energy gap between the HOMO-1 and HOMO orbitals of the neutral complexes is small (0.16-0.24 eV). The HOMO-1 has significant ligand character as well as  $\pi$ -bonding across the N–Co–N bonds thanks to effective overlap between the cobalt  $d_{yz}$  and opda  $\pi^*$  orbitals. There are obvious similarities between the HOMO-1 orbital of the neutral complexes and the singly occupied molecular orbital (SOMO) of monocationic state **[Co]<sup>+</sup>**, suggesting removal of the first electron is associated with the HOMO-1 rather than the HOMO. After coordination of the acetonitrile ligand, the SOMO is mainly the <sup>t</sup>BuUreaopda  $\pi^*$  orbital in **[3a-MeCN]<sup>+</sup>**, has significant contributions from the <sup>H</sup>opda  $\pi^*$  and cobalt  $d_{yz}$  orbitals in **[1-MeCN]<sup>+</sup>**, and has greater contributions from the cobalt  $d_{yz}$  orbital in **[5-MeCN]<sup>+</sup>**. Additional frontier molecular orbitals of the neutral complexes **1-3a**, **5**, and related oxidized species are provided in Figures S107-S111.

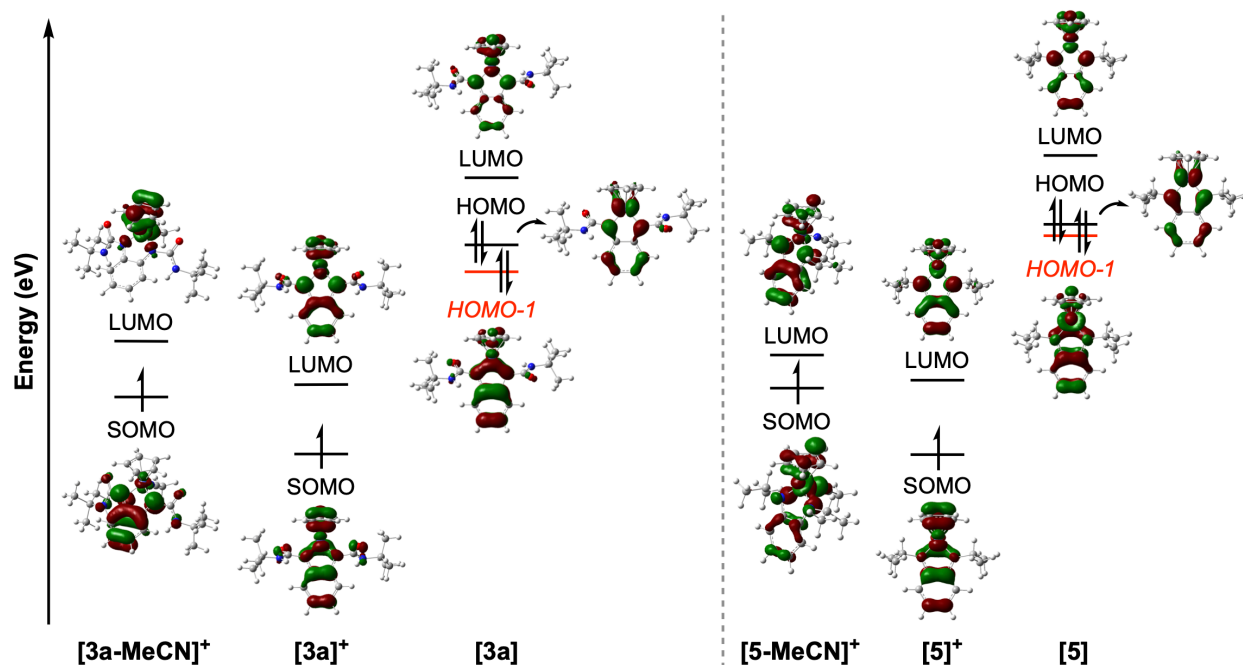


**Figure 5.** Calculated frontier molecular orbitals for **3a**, **5**, and their  $1e^-$  oxidized species.

## DISCUSSION

The phenylenediamide ligand and related O-, N-, and S-donor versions have been extensively explored over the past four decades.<sup>27-28</sup> While many reports have focused on homoleptic systems, the neutral [CpM(opda)]-type complexes have been shown to possess unique electrochemical properties that depend on the metal identity and the nature of the ligand. For [Cp\*Ir] complexes containing an amidophenolate or diphenyl-opda ligand, two distinct 1e<sup>-</sup> oxidation waves are observed by CV, while the monophenyl-opda analogue exhibits a 2e<sup>-</sup> oxidation at slower scan rates.<sup>61-63</sup> All three iridium complexes were formally assigned as Ir<sup>III</sup> with a dianionic opda (or related) ligand, and thus the oxidation processes are thought to be ligand-based. Related half-sandwich complexes of rhodium are also assigned as coordinatively unsaturated species with formal Rh<sup>III</sup> centers based on structural analysis.<sup>64-66</sup> Recently, Sarkar and co-workers reported a series of [Cp\*Rh] complexes where the CV behavior varies with the opda substituents: electron-poor sulfonyl derivatives showed 1e<sup>-</sup> waves, while the electron-rich mono- and diphenyl versions undergo a 2e<sup>-</sup> oxidation.<sup>66</sup> In contrast, previous discussions on [CpCo] or [Cp\*Co] analogues have been dominated by the Co<sup>I</sup>-bqdi assignment,<sup>41-45</sup> despite the close similarities of the N-C<sub>phenylene</sub> bond lengths to reported values for M-s-bqdi and M-opda complexes.<sup>18,31-32</sup> Furthermore, oxidation of these cobalt complexes has only been reported in passing.<sup>44,45</sup> This is surprising given that comparisons of properties across the different oxidation states of a system can be a valuable tool for revealing the nature of the electronic structure,<sup>36</sup> and the doubly-oxidized complexes in this series are reasonably expected to be Co<sup>III</sup>-bqdi, a formal Co<sup>III</sup> center with a fully oxidized bqdi ligand. The ambiguity associated with this oxidation process motivated our further study into this family, with the aim to better illuminate the electronic structure of the neutral complexes through direct comparison with their 2e<sup>-</sup> oxidized counterparts.

In all cases, the neutral cobalt complexes can be readily oxidized with mild chemical oxidants. Two equivalents of oxidant are required for complete conversion to the doubly-oxidized species; however, treatment with fewer equivalents does not lead to a 1e<sup>-</sup> oxidized intermediate. This behavior is in agreement with our electrochemical results: the peak-to-peak separation for the oxidation wave at slow scan rates is consistently smaller than the ideal value for a Nernstian 1e<sup>-</sup> process, and in many cases approaches the ideal 2e<sup>-</sup> value (29 mV). Such potential inversion is observed when the intermediate oxidation state is unstable with respect to disproportionation. The larger peak currents associated with the oxidation wave are also indicative of a 2e<sup>-</sup> wave. Thus,

we find that the previous assignment for the oxidation of **1** and the related perfluoro analogue as a  $1e^-$  process is inappropriate.<sup>44-45</sup>

As expected, the structural metrics of the doubly-oxidized complexes **1<sup>ox</sup>**-**5<sup>ox</sup>** are in line with a  $[\text{Cp}^{\text{R}'}\text{Co}^{\text{III}}(\text{R}^{\text{bqdi}})(\text{MeCN})]^{2+}$  formulation.<sup>67</sup> In particular, the  $\text{N}-\text{C}_{\text{phenylene}}$  bond lengths are  $1.30 \pm 0.01 \text{ \AA}$ , which is typical of  $\text{C}=\text{N}$  bonds in metal-diimine systems. The phenylene backbone also shows a non-aromatic quinone structure with alternating single and double bonds. The bqdi ligand is a weaker  $\sigma$ -donor than the reduced forms (s-bqdi or opda), which likely contributes to the facile ligand loss observed in solution for the oxidized complexes under certain conditions. We found this to be especially problematic for the electron-deficient ureayl derivatives **3a-3d** and **4**, though this is likely partially compensated by greater  $\pi$ -backdonation to the oxidized ligand.<sup>34</sup> Complexes **1<sup>ox</sup>**-**5<sup>ox</sup>** are also diamagnetic and show no evidence of paramagnetic broadening by NMR, consistent with an  $18e^-$ , coordinatively saturated electronic description based on a low-spin  $\text{Co}^{\text{III}}$  center in a pseudo-octahedral geometry.

With the unambiguous characterization of the oxidized species, we turn our focus to the neutral complexes **1-5**. Although formal oxidation state assignments may be inappropriate due to the non-innocent nature of the phenylenediamide ligand, our experimental and computational results can rule out one possibility. A formal  $\text{Co}^{\text{I}}$  center with a bqdi ligand is excluded based on the significant structural differences between the neutral and oxidized complexes. Most notably, the substantial decrease in  $\text{N}-\text{C}_{\text{phenylene}}$  bond lengths and the clear decrease in phenylene aromaticity upon oxidation indicate some degree of ligand-based oxidation. This conclusion is further supported by the  $^1\text{H}$  NMR chemical shift of the NH resonance for **2**, which is upfield compared to the diimine NH signal of **2<sup>ox</sup>** and again signifies a more reduced ligand in **2**. Thus, we conclude that the previous  $\text{Co}^{\text{I}}$ -bqdi assignment for this family of complexes should be revised.

At the same time, the solid-state structures of **1-5** are not fully consistent with a formal  $\text{Co}^{\text{III}}$  description and dianionic opda ligand, in which the  $\text{N}-\text{C}_{\text{phenylene}}$  single bond lengths are typically closer to  $1.40 \text{ \AA}$  and the  $\text{C}-\text{C}$  bond lengths in the phenylene backbone are identical.<sup>18,31,33</sup> Instead, the intermediate  $\text{N}-\text{C}_{\text{phenylene}}$  bond lengths in **1-5** may suggest a semiquinone-type radical anion (s-bqdi). Given the diamagnetism of these complexes, a ligand radical must be strongly antiferromagnetically coupled to a low-spin  $\text{Co}^{\text{II}}$  center, i.e., a  $\text{Co}^{\text{II}}$ -s-bqdi description ( $S_{\text{total}} = 0$ ). An alternative explanation is a closed-shell system with no radical character: covalent  $\pi$ -bonding or resonance delocalization across the metallocycle may instead give rise to the observed bond

metrics. Our DFT calculations suggest the latter is more reasonable. While we were able to obtain the calculated structure of the antiferromagnetically coupled biradical of **3a** using hybrid functionals, these calculations do not predict a  $2e^-$  oxidation and thus were not explored further. However, potential inversion is accurately reproduced for the closed-shell singlet using the BP86 functional, which also matched well with our other characterization data. Thus, we consider this functional capable of modeling the electronic structure of these complexes. The calculated HOMO of each neutral complex is the  $\pi^*$ -antibonding combination of the cobalt  $d_{xy}$  and ligand  $\pi$  orbitals, which is typical for coordinatively saturated late transition metal centers with  $\pi$ -donor ligands such as amides ( $NR_2^-$ ). The HOMO-1 is the  $\pi$ -bonding combination of the cobalt  $d_{yz}$  and ligand  $\pi^*$  orbitals, highlighting the covalent nature of this interaction. Overall, we describe these complexes as having delocalized bonding with resonance stabilization across the metallocycle and effective overlap between the metal  $d$  orbitals and the  $\pi$ -system of the opda ligand.

The observation of a  $2e^-$  process in a single CV wave is rare at first-row transition metal complexes containing one metal center and one redox-active ligand.<sup>21-23</sup> For **1**, **3a**, and **5**, the  $2e^-$  oxidation is initiated by loss of one electron to yield a low-spin  $Co^{II}$  species, based on DFT. Complex [**2**]<sup>+</sup> is predicted to have spin density on both the metal and ligand, likely due to the increased electron-donating character of the  $Cp^*$  ligand. In each case, the calculated structural changes concomitant with the first electron transfer indicate a decrease in electron density at the ligand, resulting in structures that bear more resemblance to the diimine description. Thus, this intermediate state may be approximately viewed as  $[Cp^{R'}Co^{II}(Rbqdi)]^+$  systems, formed via ligand oxidation and redox-induced electron transfer to cobalt.<sup>68-70</sup> The first electron loss appears to involve the HOMO-1 of the neutral complexes, which has significant ligand  $\pi^*$  contributions and is consistent with our assignment of this process being ligand-based. Such behavior may occur when conformational changes accompany a redox process, leading to an associated reordering of the HOMO and HOMO-1.<sup>71</sup> Here, the close energies of the HOMO and HOMO-1 orbitals and the predicted structural changes upon  $1e^-$  oxidation may be responsible for this orbital reordering.

Loss of the second electron is facile after coordination of an acetonitrile ligand, leading to the remarkable situation where  $E_2 < E_1$  regardless of the ligand substituents in this series. While acetonitrile coordination is calculated to be slightly uphill for each case, all values are energetically accessible at ambient conditions. Similar equilibria have been proposed for other  $[CpCo^{II}]$  systems.<sup>72-73</sup> Importantly, solvent coordination only becomes accessible following the first electron

loss. The accompanying increase in the ligand oxidation state results in weakened cobalt-ligand bonding and decreased aromaticity of the metallocycle, as evidenced by the calculated DFT structures. These factors lead to distortion of the T-shaped geometry and prime the cobalt center for additional ligand coordination. Without the acetonitrile ligand, further oxidation of  $[\text{Cp}^{\text{R}'}\text{Co}^{\text{II}}(\text{R}^{\text{bqdi}})]^+$  would occur at a significantly more positive potential (Scheme 3). The resulting species,  $[\text{Cp}^{\text{R}'}\text{Co}^{\text{III}}(\text{R}^{\text{bqdi}})]^{2+}$ , would consist of a coordinatively unsaturated  $\text{Co}^{\text{III}}$  center and neutral bqdi ligand. The acetonitrile ligand is predicted to provide significant stabilization to this high-energy species (Table S33), offsetting the electrostatic penalty of  $2e^-$  oxidation. Thus, the change in geometry via an *ECE* pathway is crucial for accessing the second electron transfer at mild potentials and enabling the potential inversion.

The location of the second electron transfer depends on the phenylenediamide substituents. Looking at the  $^{\text{H}}\text{opda}$ ,  $^{\text{tBuUrea}}\text{opda}$ , and  $^{\text{iPr}}\text{opda}$  systems, there are clear differences in the calculated spin density of the  $[\text{Co-MeCN}]^+$  intermediate. The withdrawing nature of the  $^{\text{tBuUrea}}\text{opda}$  ligand pulls the unpaired spin density away from the metal and onto the ligand upon acetonitrile coordination; consequently,  $[\mathbf{3a-MeCN}]^+$  may be described as a  $\text{Co}^{\text{III}}\text{-s-bqdi}$  system and its  $1e^-$  oxidation to  $\mathbf{3a}^{\text{ox}}$  is ligand-based. On the other hand, the donating  $^{\text{iPr}}\text{opda}$  ligand pushes the unpaired spin density toward cobalt, maintaining the  $\text{Co}^{\text{II}}\text{-bqdi}$  description in  $[\mathbf{5-MeCN}]^+$  and leading to the second electron loss being metal-based. These trends are also seen in the orbital contributions to the SOMO orbital for the  $[\text{Co-MeCN}]^+$  species. Overall, greater electron-withdrawing character at the ligand favors two ligand-based oxidations (from the  $\pi^*$  orbital), while greater electron-donating character favors one ligand ( $\pi^*$ ) and one metal ( $d_{yz}$ ) oxidation (Figure 6). We note that  $\mathbf{2}$  does not directly align in this trend due to contributions from the electron-rich  $\text{Cp}^*$  ligand – this system shows significant ligand involvement in the frontier molecular orbitals and spin density for  $[\mathbf{2}]^+$  and  $[\mathbf{2-MeCN}]^+$ . Remarkably, despite these differences, all complexes in this study show potential inversion. Our results suggest that further tuning of the ligand properties may be employed to access a larger potential range for the  $2e^-$  oxidation through redistribution of electron density across the metal  $d$  and ligand  $\pi^*$  orbitals. Efforts to establish the limits of this redox tuning and consequences for reactivity are currently underway in our group.

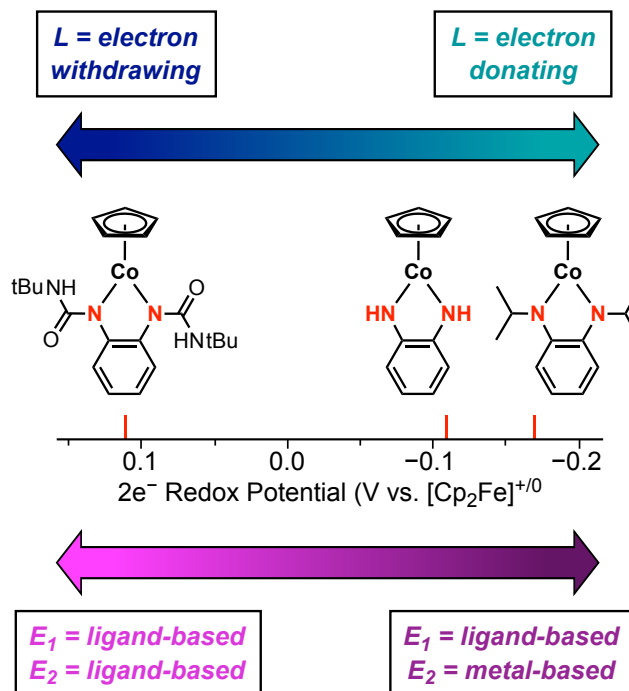


**Figure 6.** Changes in the sites of  $2e^-$  oxidation for **1**, **3a**, and **5** as a function of electronic character of the phenylenediamide ligand.

Reports demonstrating multielectron processes over a series of first-row transition metal complexes with different ligand properties are extremely scarce.<sup>74-75</sup> With **1-5**, we are not only able to tune the potential at which the  $2e^-$  oxidation occurs by more than 0.5 V, but also control the formal sites of oxidation. The importance of structural reorganization for multielectron redox behavior has been noted.<sup>3-4</sup> Here, the initial ligand-based oxidation and associated geometry changes are critical to accessing the potential inversion, generating a coordinatively unsaturated  $[\text{Cp}^{\text{R}'}\text{Co}^{\text{II}}(\text{R}^{\text{b}}\text{qdi})]^+$  intermediate that can interact with an incoming ligand (i.e., acetonitrile). Remarkably, reversible CV behavior is maintained in THF and DCM – it is only with a non-coordinating electrolyte anion ( $\text{BArF}_{24}^-$ ) and non-coordinating solvent do we observe any noteworthy loss of reversibility for select complexes. This behavior indicates that sufficient stabilization of the dicationic state can be provided by species other than acetonitrile, pointing to the possibility of forming other Co–X bonds through reactivity with different reagents.

## CONCLUSION

Despite several years of investigations into metal-phenylenediamide complexes, the electronic structure and oxidation behavior of the half-sandwich complexes  $[\text{Cp}^{\text{R}'}\text{Co}^{\text{R}}\text{opda}]$  has yet to be fully elucidated. In this report, we have investigated several examples in this family and shown that all complexes undergo a  $2e^-$  oxidation regardless of the opda substituents. These complexes have significant  $\pi$ -delocalization across the cobalt-opda metallocycle thanks to effective energy matching of the cobalt  $d$  and ligand  $\pi^*$  orbitals. Following an *ECE* mechanism for oxidation, loss of the first electron occurs from the ligand, which disrupts the resonance conjugation in the metallocycle and destabilizes the T-shaped geometry, facilitating structural reorganization. Coordination of an acetonitrile ligand in the chemical step preferentially stabilizes the dicationic state, resulting in potential inversion and an overall  $2e^-$  process. Notably, the electronic properties of the phenylenediamide ligand not only affect the  $2e^-$  oxidation potential but also control the site of the second electron transfer step. This novel behavior offers the unique opportunity to tune the phenylenediamide ligand to control the reactivity at cobalt, while promoting multielectron transformations through cooperative metal-ligand electron storage. In this context, we are currently exploring the reactivity of these cobalt complexes toward electrophilic addition promoted by the phenylenediamide ligand.

## ASSOCIATED CONTENT

### Supporting Information

The following files are available free of charge.

- Experimental procedures, crystallographic details, NMR spectra, cyclic voltammetry (CV) studies, electronic absorption spectra, computational results, and Cartesian coordinates for DFT calculated structures (PDF)

### Accession Codes

CDCC 2183201-2183205 and 2183207-2183213 contain the supplemental crystallographic data for this paper. These data can be obtained free of charge via [www.ccdc.cam.ac.uk/data\\_request/cif](http://www.ccdc.cam.ac.uk/data_request/cif), or by emailing [data\\_request@ccdc.cam.ac.uk](mailto:data_request@ccdc.cam.ac.uk), or by contacting The Cambridge Crystallographic Data Centre, 12 Union Road, Cambridge CB2 1EZ, UK; fax: +44 1223 336033.

## **AUTHOR INFORMATION**

### **Corresponding Author**

**Kate M. Waldie** - Department of Chemistry and Chemical Biology, Rutgers, The State University of New Jersey, Piscataway, New Jersey 08854, United States; orcid.org/0000-0001-6444-6122; E-mail: [kate.waldie@rutgers.edu](mailto:kate.waldie@rutgers.edu)

### **Authors**

**Minzhu Zou** - Department of Chemistry and Chemical Biology, Rutgers, The State University of New Jersey, Piscataway, New Jersey 08854, United States; orcid.org/0000-0002-2710-135X

**Thomas J. Emge** - Department of Chemistry and Chemical Biology, Rutgers, The State University of New Jersey, Piscataway, New Jersey 08854, United States

### **Author Contributions**

M.Z. carried out the syntheses, characterizations, and calculations of the reported complexes. The crystal structure data collection and analyses were performed by T.J.E and M.Z. The project was supervised by K.M.W., and the manuscript was written and edited by M.Z. and K.M.W. All authors have given approval to the final version of the manuscript.

### **NOTES**

The authors declare no competing financial interests.

### **ACKNOWLEDGMENTS**

The authors gratefully acknowledge financial support from the ACS Petroleum Research Fund (65171-DNI3) and Rutgers, The State University of New Jersey. The authors acknowledge the Office of Advanced Research Computing (OARC) at Rutgers, The State University of New Jersey for providing access to the Amarel cluster and associated research computing resources that have contributed to the results reported here. The authors acknowledge Professor Roger A. Lalancette, Department of Chemistry, Rutgers University, Newark, NJ 07102 for additional X-ray data collection and discussions on the structure refinement.

## REFERENCES

1. Zell, T.; Langer, R., From Ruthenium to Iron and Manganese—A Mechanistic View on Challenges and Design Principles of Base-Metal Hydrogenation Catalysts. *ChemCatChem* **2018**, *10* (9), 1930-1940. DOI: 10.1002/cctc.201701722
2. Evans, D. H., One-Electron and Two-Electron Transfers in Electrochemistry and Homogeneous Solution Reactions. *Chem. Rev.* **2008**, *108* (7), 2113-2144. DOI: 10.1021/cr068066l
3. Macías-Ruvalcaba, N. A.; Evans, D. H., Electron Transfer and Structural Change: Distinguishing Concerted and Two-Step Processes. *Chem. Eur. J.* **2007**, *13* (16), 4386-4395. DOI: 10.1002/chem.200700338
4. Fortage, J.; Peltier, C.; Perruchot, C.; Takemoto, Y.; Teki, Y.; Bedioui, F.; Marvaud, V.; Dupeyre, G.; Pospíšil, L.; Adamo, C.; Hromadová, M.; Ciofini, I.; Lainé, P. P., Single-Step versus Stepwise Two-Electron Reduction of Polyarylpiperidiniums: Insights from the Steric Switching of Redox Potential Compression. *J. Am. Chem. Soc.* **2012**, *134* (5), 2691-2705. DOI: 10.1021/ja210024y
5. Bullock, R. M., Reaction: Earth-Abundant Metal Catalysts for Energy Conversions. *Chem* **2017**, *2* (4), 444-446. DOI: 10.1016/j.chempr.2017.03.019
6. Ludwig, J. R.; Schindler, C. S., Catalyst: Sustainable Catalysis. *Chem* **2017**, *2* (3), 313-316. DOI: 10.1016/j.chempr.2017.02.014
7. Arevalo, R.; Chirik, P. J., Enabling Two-Electron Pathways with Iron and Cobalt: From Ligand Design to Catalytic Applications. *J. Am. Chem. Soc.* **2019**, *141* (23), 9106-9123. DOI: 10.1021/jacs.9b03337
8. Bullock, R. M.; Chen, J. G.; Gagliardi, L.; Chirik, P. J.; Farha, O. K.; Hendon, C. H.; Jones, C. W.; Keith, J. A.; Klosin, J.; Minter, S. D.; Morris, R. H.; Radosevich, A. T.; Rauchfuss, T. B.; Strotman, N. A.; Vojvodic, A.; Ward, T. R.; Yang, J. Y.; Surendranath, Y., Using nature's blueprint to expand catalysis with Earth-abundant metals. *Science* **2020**, *369* (6505), eabc3183. DOI: 10.1126/science.abc3183
9. Wu, T.; Rajabimoghadam, K.; Puri, A.; Hebert, D. D.; Qiu, Y. L.; Eichelberger, S.; Siegler, M. A.; Swart, M.; Hendrich, M. P.; Garcia-Bosch, I., A 4H<sup>+</sup>/4e<sup>-</sup> Electron-Coupled-Proton Buffer Based on a Mononuclear Cu Complex. *J. Am. Chem. Soc.* **2022**, *144* (37), 16905-16915. DOI: 10.1021/jacs.2c05454
10. Chirik, P. J.; Wieghardt, K., Radical Ligands Confer Nobility on Base-Metal Catalysts. *Science* **2010**, *327* (5967), 794-795. DOI: 10.1126/science.1183281
11. Kaim, W., Manifestations of Noninnocent Ligand Behavior. *Inorg. Chem.* **2011**, *50* (20), 9752-9765. DOI: 10.1021/ic2003832
12. Lyaskovskyy, V.; de Bruin, B., Redox Non-Innocent Ligands: Versatile New Tools to Control Catalytic Reactions. *ACS Catal.* **2012**, *2* (2), 270-279. DOI: 10.1021/cs200660v
13. van der Vlugt, J. I., Radical-Type Reactivity and Catalysis by Single-Electron Transfer to or from Redox-Active Ligands. *Chem. Eur. J.* **2019**, *25* (11), 2651-2662. DOI: 10.1002/chem.201802606

14. van Leest, N. P.; de Zwart, F. J.; Zhou, M.; de Bruin, B., Controlling Radical-Type Single-Electron Elementary Steps in Catalysis with Redox-Active Ligands and Substrates. *JACS Au* **2021**, *1* (8), 1101-1115. DOI: 10.1021/jacsau.1c00224
15. Whittaker, J. W., Free Radical Catalysis by Galactose Oxidase. *Chem. Rev.* **2003**, *103* (6), 2347-2364. DOI: 10.1021/cr020425z
16. Richert, S. A.; Tsang, P. K. S.; Sawyer, D. T., Ligand-Centered Redox Processes for  $MnL_3$ ,  $FeL_3$ , and  $CoL_3$  Complexes (L = Acetylacetonate, 8-Quinolate, Picolinate, 2,2'-Bipyridyl, 1,10-Phenanthroline) and for Their Tetrakis(2,6-dichlorophenyl)porphinato Complexes [M(Por)]. *Inorg. Chem.* **1989**, *28* (12), 2471-2475. DOI: 10.1021/ic00311a044
17. Bartlett, P. N.; Eastwick-Field, V., A reinvestigation of the electrochemistry of  $[Ni^{(II)}(bpy)_3(ClO_4)_2]$  in acetonitrile using rotating disc and rotating ring-disc electrodes. *Electrochim. Acta* **1993**, *38* (17), 2515-2523. DOI: 10.1016/0013-4686(93)80147-r
18. Chlopek, K.; Bothe, E.; Neese, F.; Weyhermuller, T.; Wieghardt, K., Molecular and Electronic Structures of Tetrahedral Complexes of Nickel and Cobalt Containing *N,N'*-Disubstituted, Bulky *o*-Diiminobenzosemiquinonate(1-)  $\pi$ -Radical Ligands. *Inorg. Chem.* **2006**, *45* (16), 6298-6307. DOI: 10.1021/ic060242l
19. Ghosh, P.; Samanta, S.; Roy, S. K.; Joy, S.; Krämer, T.; McGrady, J. E.; Goswami, S., Redox Noninnocence in Coordinated 2-(Arylazo)pyridines: Steric Control of Ligand-Based Redox Processes in Cobalt Complexes. *Inorg. Chem.* **2013**, *52* (24), 14040-14049. DOI: 10.1021/ic4018079
20. Sengupta, D.; Ghosh, P.; Chatterjee, T.; Datta, H.; Paul, N. D.; Goswami, S., Ligand-Centered Redox in Nickel(II) Complexes of 2-(Arylazo)pyridine and Isolation of 2-Pyridyl-Substituted Triaryl Hydrazines via Catalytic N-Arylation of Azo-Function. *Inorg. Chem.* **2014**, *53* (22), 12002-12013. DOI: 10.1021/ic501656s
21. Sampson, M. D.; Nguyen, A. D.; Grice, K. A.; Moore, C. E.; Rheingold, A. L.; Kubiak, C. P., Manganese Catalysts with Bulky Bipyridine Ligands for the Electrocatalytic Reduction of Carbon Dioxide: Eliminating Dimerization and Altering Catalysis. *J. Am. Chem. Soc.* **2014**, *136* (14), 5460-5471. DOI: 10.1021/ja501252f
22. Waldie, K. M.; Ramakrishnan, S.; Kim, S.-K.; Maclaren, J. K.; Chidsey, C. E. D.; Waymouth, R. M., Multielectron Transfer at Cobalt: Influence of the Phenylazopyridine Ligand. *J. Am. Chem. Soc.* **2017**, *139* (12), 4540-4550. DOI: 10.1021/jacs.7b01047
23. Matson, B. D.; McLoughlin, E. A.; Armstrong, K. C.; Waymouth, R. M.; Sarangi, R., Effect of Redox Active Ligands on the Electrochemical Properties of Manganese Tricarbonyl Complexes. *Inorg. Chem.* **2019**, *58* (11), 7453-7465. DOI: 10.1021/acs.inorgchem.9b00652
24. Richburg, C. S.; Farnum, B. H., Influence of Pyridine on the Multielectron Redox Cycle of Nickel Diethyldithiocarbamate. *Inorg. Chem.* **2019**, *58* (22), 15371-15384. DOI: 10.1021/acs.inorgchem.9b02430
25. Mazumder, M. M. R.; Burton, A.; Richburg, C. S.; Saha, S.; Cronin, B.; Duin, E.; Farnum, B. H., Controlling One-Electron vs Two-Electron Pathways in the Multi-Electron Redox Cycle of Nickel Diethyldithiocarbamate. *Inorg. Chem.* **2021**, *60* (17), 13388-13399. DOI: 10.1021/acs.inorgchem.1c01699

26. Bamberger, H.; Albold, U.; Dubnická Midlíková, J.; Su, C.-Y.; Deibel, N.; Hunger, D.; Hallmen, P. P.; Neugebauer, P.; Beerhues, J.; Demeshko, S.; Meyer, F.; Sarkar, B.; van Slageren, J., Iron(II), Cobalt(II), and Nickel(II) Complexes of Bis(sulfonamido)benzenes: Redox Properties, Large Zero-Field Splittings, and Single-Ion Magnets. *Inorg. Chem.* **2021**, *60* (5), 2953-2963. DOI: 10.1021/acs.inorgchem.0c02949
27. Broere, D. L. J.; Plessius, R.; van der Vlugt, J. I., New avenues for ligand-mediated processes – expanding metal reactivity by the use of redox-active catechol, *o*-aminophenol and *o*-phenylenediamine ligands. *Chem. Soc. Rev.* **2015**, *44* (19), 6886-6915. DOI: 10.1039/c5cs00161g
28. Rajput, A.; Sharma, A. K.; Barman, S. K.; Saha, A.; Mukherjee, R., Valence tautomerism and delocalization in transition metal complexes of *o*-amidophenolates and other redox-active ligands. Some recent results. *Coord. Chem. Rev.* **2020**, *414*, 213240. DOI: 10.1016/j.ccr.2020.213240
29. Chaudhuri, P.; Verani, C. N.; Bill, E.; Bothe, E.; Weyhermüller, T.; Wieghardt, K., Electronic Structure of Bis(*o*-iminobenzosemiquinonato)metal Complexes (Cu, Ni, Pd). The Art of Establishing Physical Oxidation States in Transition-Metal Complexes Containing Radical Ligands. *J. Am. Chem. Soc.* **2001**, *123* (10), 2213-2223. DOI: 10.1021/ja003831d
30. Pierpont, C. G., Studies on charge distribution and valence tautomerism in transition metal complexes of catecholate and semiquinonate ligands. *Coord. Chem. Rev.* **2001**, *216-217*, 99-125. DOI: 10.1016/s0010-8545(01)00309-5
31. Herebian, D.; Bothe, E.; Neese, F.; Weyhermüller, T.; Wieghardt, K., Molecular and Electronic Structures of Bis(*o*-diiminobenzosemiquinonato)metal(II) Complexes (Ni, Pd, Pt), Their Monocations and -Anions, and of Dimeric Dications Containing Weak Metal–Metal Bonds. *J. Am. Chem. Soc.* **2003**, *125* (30), 9116-9128. DOI: 10.1021/ja030123u
32. Bill, E.; Bothe, E.; Chaudhuri, P.; Chlopek, K.; Herebian, D.; Kokatam, S.; Ray, K.; Weyhermüller, T.; Neese, F.; Wieghardt, K., Molecular and Electronic Structure of Four- and Five-Coordinate Cobalt Complexes Containing Two *o*-Phenylenediamine- or Two *o*-Aminophenol-Type Ligands at Various Oxidation Levels: An Experimental, Density Functional, and Correlated ab initio Study. *Chem. Eur. J.* **2005**, *11* (1), 204-224. DOI: 10.1002/chem.200400850
33. Ray, K.; Petrenko, T.; Wieghardt, K.; Neese, F., Joint spectroscopic and theoretical investigations of transition metal complexes involving non-innocent ligands. *Dalton Trans.* **2007**, (16), 1552-1566. DOI: 10.1039/b700096k
34. Skara, G.; Pinter, B.; Geerlings, P.; De Proft, F., Revealing the thermodynamic driving force for ligand-based reductions in quinoids; conceptual rules for designing redox active and non-innocent ligands. *Chem. Sci.* **2015**, *6* (7), 4109-4117. DOI: 10.1039/c5sc01140j
35. Skara, G.; Gimferrer, M.; De Proft, F.; Salvador, P.; Pinter, B., Scrutinizing the Noninnocence of Quinone Ligands in Ruthenium Complexes: Insights from Structural, Electronic, Energy, and Effective Oxidation State Analyses. *Inorg. Chem.* **2016**, *55* (5), 2185-2199. DOI: 10.1021/acs.inorgchem.5b02543

36. Mukherjee, R., Assigning Ligand Redox Levels in Complexes of 2-Aminophenolates: Structural Signatures. *Inorg. Chem.* **2020**, *59* (18), 12961-12977. DOI: 10.1021/acs.inorgchem.0c00240
37. Smith, A. L.; Hardcastle, K. I.; Soper, J. D., Redox-Active Ligand-Mediated Oxidative Addition and Reductive Elimination at Square Planar Cobalt(III): Multielectron Reactions for Cross-Coupling. *J. Am. Chem. Soc.* **2010**, *132* (41), 14358-14360. DOI: 10.1021/ja106212w
38. van der Meer, M.; Rechkemmer, Y.; Peremykin, I.; Hohloch, S.; van Slageren, J.; Sarkar, B., (Electro)catalytic C–C bond formation reaction with a redox-active cobalt complex. *Chem. Commun.* **2014**, *50* (76), 11104-11106. DOI: 10.1039/c4cc03309d
39. Joh, T.; Hagihara, N.; Murahashi, S., Formation of Complexes from Azobenzenes and Cyclopentadienyl Cobalt Derivatives. *Bull. Chem. Soc. Jpn.* **1967**, *40* (3), 661-664. DOI: 10.1246/bcsj.40.661
40. Gross, M. E.; Ibers, J. A.; Trogler, W. C., Structural and Spectroscopic Study of Cyclopentadienylcobalt *N*-Phenyl-*o*-Benzoquinone Diimines. A Case for Delocalized  $\pi$  Bonding. *Organometallics* **1982**, *1* (3), 530-535. DOI: 10.1021/om00063a023
41. Miller, E. J.; Brill, T. B., The metal atom's view of the bonding in *o*-benzoquinone, *o*-dithiobenzoquinone, and *o*-benzoquinone diimine metallacycles of  $(\eta^5\text{-C}_5\text{H}_5)\text{Co}$ . A  $^{59}\text{Co}$  NQR study of the *cis*- $a_3b_2$  ligand geometry. *Inorg. Chem.* **1983**, *22* (17), 2392-2398. DOI: 10.1021/ic00159a011
42. Rheingold, A. L.; Fultz, W. C.; Brill, T. B.; Landon, S. J., Crystal and molecular structure of  $(\eta^5\text{-C}_5\text{H}_5)\text{Co}(\text{HNC}_6\text{H}_4\text{NH})$ , a cobalt *o*-quinonediimine complex. *J. Crystallogr. Spectrosc. Res.* **1983**, *13* (5), 317-323. DOI: 10.1007/bf01161295
43. Miller, E. J.; Rheingold, A. L.; Brill, T. B., Bonding and structure in cyclopentadienylcobaltmetallacycle complexes. The crystal structures of  $[\eta^5\text{-C}_5(\text{CH}_3)_5]\text{Co}[(\text{NH})_2\text{C}_6\text{H}_4]$  and  $[\eta^5\text{-C}_5(\text{CH}_3)_5]\text{Co}[(\text{NH})\text{SC}_6\text{H}_4]$ . *J. Organomet. Chem.* **1985**, *282* (3), 399-412. DOI: 10.1016/0022-328x(85)87198-9
44. Reinhardt, M.; Dalglish, S.; Shuku, Y.; Reissig, L.; Matsushita, M. M.; Crain, J.; Awaga, K.; Robertson, N., Molecular and thin film properties of cobalt half-sandwich compounds for optoelectronic application. *Phys. Chem. Chem. Phys.* **2017**, *19* (9), 6768-6776. DOI: 10.1039/c6cp08685c
45. Pilia, L.; Shuku, Y.; Dalglish, S.; Hofmann, D. W. M.; Melis, N.; Awaga, K.; Robertson, N., Effect of fluorination on the crystal and electronic structure of organometallic cyclopentadienyl-phenylenediamino-cobalt complexes. *J. Organomet. Chem.* **2020**, *918*, 121277. DOI: 10.1016/j.jorganchem.2020.121277
46. Štrukil, V.; Margetić, D.; Igrc, M. D.; Eckert-Maksić, M.; Friščić, T., Desymmetrisation of aromatic diamines and synthesis of non-symmetrical thiourea derivatives by click-mechanochemistry. *Chem. Commun.* **2012**, *48* (78), 9705-9707. DOI: 10.1039/c2cc34013e
47. Ould, D. M. C.; Rigby, A. C.; Wilkins, L. C.; Adams, S. J.; Platts, J. A.; Pope, S. J. A.; Richards, E.; Melen, R. L., Investigations into the Photophysical and Electronic Properties of Pnictoles and Their Pnictenium Counterparts. *Organometallics* **2017**, *37* (5), 712-719. DOI: 10.1021/acs.organomet.7b00564

48. Rajabimoghadam, K.; Darwish, Y.; Bashir, U.; Pitman, D.; Eichelberger, S.; Siegler, M. A.; Swart, M.; Garcia-Bosch, I., Catalytic Aerobic Oxidation of Alcohols by Copper Complexes Bearing Redox-Active Ligands with Tunable H-Bonding Groups. *J. Am. Chem. Soc.* **2018**, *140* (48), 16625-16634. DOI: 10.1021/jacs.8b08748
49. Heck, R. F., Cyclopentadienylcobalt Derivatives of Chelating Aromatic Ligands. *Inorg. Chem.* **1968**, *7* (8), 1513-1516. DOI: 10.1021/ic50066a009
50. Miller, E. J.; Landon, S. J.; Brill, T. B.,  $\eta^5$ -C<sub>5</sub>(CH<sub>3</sub>)<sub>5</sub> vs.  $\eta^5$ -C<sub>5</sub>H<sub>5</sub>. A Comparison of Electronic Influences for Metallocenes with *fac*-a<sub>3</sub>b<sub>2</sub>c, *fac*-a<sub>3</sub>b<sub>3</sub>, and *cis*-a<sub>3</sub>b<sub>2</sub> Ligand Geometry Based on <sup>59</sup>Co NQR Spectroscopy. *Organometallics* **1985**, *4* (3), 533-538, DOI: 10.1021/om00122a018.
51. Connelly, N. G.; Geiger, W. E., Chemical Redox Agents for Organometallic Chemistry. *Chem. Rev.* **1996**, *96* (2), 877-910. DOI: 10.1021/cr940053x
52. Kuhn, N.; Brüggemann, H.; Winter, M.; De Bellis, V. M., Synthese und reaktivität von dienylmetall-verbindingen: XXVII. Ein einfacher weg zur synthese von cyclopentadienylcobalt(III)-dikationen. *J. Organomet. Chem.* **1987**, *320* (3), 391-400. DOI: 10.1016/0022-328x(87)85062-3
53. Avilés, T.; Dinis, A.; Calhorda, M. J.; Pinto, P. c.; Félix, V.; Drew, M. G. B., Synthesis, X-ray structure, and theoretical studies of novel cationic mono-cyclopentadienyl complexes of Co(III): the orthometalation of *trans*-azobenzene. *J. Organomet. Chem.* **2001**, *625* (2), 186-194. DOI: 10.1016/s0022-328x(00)00948-7
54. Waldie, K. M.; Kim, S.-K.; Ingram, A. J.; Waymouth, R. M., Cyclopentadienyl Cobalt Complexes as Precatalysts for Electrocatalytic Hydrogen Evolution. *Eur. J. Inorg. Chem.* **2017**, *2017* (20), 2755-2761. DOI: 10.1002/ejic.201700188
55. Metcalfe, R. A.; Lever, A. B. P., Tetraammineruthenium(II) and -ruthenium(III) Complexes of *o*-Benzoquinone Diimine and Their Redox Series. *Inorg. Chem.* **1997**, *36* (21), 4762-4771. DOI: 10.1021/ic970236c
56. Bard, A. J.; Faulkner, L. R., Electrode Reactions with Coupled Homogeneous Chemical Reactions. In *Electrochemical Methods: Fundamentals and Applications*, 2nd ed.; John Wiley & Sons, 2001; pp 471-533.
57. Smith, A. L.; Clapp, L. A.; Hardcastle, K. I.; Soper, J. D., Redox-active ligand-mediated Co-Cl bond-forming reactions at reducing square planar cobalt(III) centers. *Polyhedron* **2010**, *29* (1), 164-169. DOI: 10.1016/j.poly.2009.06.046
58. Minkin, V. I.; Starikov, A. G.; Starikova, A. A., Computational insight into magnetic behavior and properties of the transition metal complexes with redox-active ligands: a DFT approach. *Pure Appl. Chem.* **2018**, *90* (5), 811-824. DOI: 10.1515/pac-2017-0803
59. Roy, L. E.; Jakubikova, E.; Guthrie, M. G.; Batista, E. R., Calculation of One-Electron Redox Potentials Revisited. Is It Possible to Calculate Accurate Potentials with Density Functional Methods? *J. Phys. Chem. A* **2009**, *113* (24), 6745-6750. DOI: 10.1021/jp811388w
60. Herebian, D.; Wieghardt, K. E.; Neese, F., Analysis and Interpretation of Metal-Radical Coupling in a Series of Square Planar Nickel Complexes: Correlated Ab Initio and Density Functional Investigation of [Ni(L<sup>ISQ</sup>)<sub>2</sub>] (L<sup>ISQ</sup>=3,5-di-*tert*-butyl-*o*-

- diiminobenzosemiquinonate(1-)). *J. Am. Chem. Soc.* **2003**, *125* (36), 10997-11005. DOI: 10.1021/ja030124m
61. Ringenberg, M. R.; Kokatam, S. L.; Heiden, Z. M.; Rauchfuss, T. B., Redox-Switched Oxidation of Dihydrogen Using a Non-Innocent Ligand. *J. Am. Chem. Soc.* **2008**, *130* (3), 788-789. DOI: 10.1021/ja076801k
62. van der Meer, M.; Manck, S.; Sobottka, S.; Plebst, S.; Sarkar, B., Redox Activity and Bond Activation in Iridium–Diamidobenzene Complexes: A Combined Structural, (Spectro)electrochemical, and DFT Investigation. *Organometallics* **2015**, *34* (22), 5393-5400. DOI: 10.1021/acs.organomet.5b00716
63. Sobottka, S.; van der Meer, M. B.; Glais, E.; Albold, U.; Suhr, S.; Su, C.-Y.; Sarkar, B., A coordinatively unsaturated iridium complex with an unsymmetrical redox-active ligand: (spectro)electrochemical and reactivity studies. *Dalton Trans.* **2019**, *48* (37), 13931-13942. DOI: 10.1039/c9dt01597c
64. Blacker, A. J.; Clot, E.; Duckett, S. B.; Eisenstein, O.; Grace, J.; Nova, A.; Perutz, R. N.; Taylor, D. J.; Whitwood, A. C., Synthesis and structure of “16-electron” rhodium(III) catalysts for transfer hydrogenation of a cyclic imine: mechanistic implications. *Chem. Commun.* **2009**, (44), 6801-6803. DOI: 10.1039/b912943j
65. Fujita, D.; Kaga, A.; Sugimoto, H.; Morimoto, Y.; Itoh, S., Controlling Coordination Number of Rhodium(III) Complex by Ligand-Based Redox for Catalytic C–H Amination. *Bull. Chem. Soc. Jpn.* **2020**, *93* (2), 279-286. DOI: 10.1246/bcsj.20190291
66. Suhr, S.; Walter, R.; Beerhues, J.; Albold, U.; Sarkar, B., Rhodium diamidobenzene complexes: a tale of different substituents on the diamidobenzene ligand. *Chem. Sci.* **2022**, *13* (35), 10532-10545. DOI: 10.1039/d2sc03227a
67. Bugarcic, T.; Habtemariam, A.; Deeth, R. J.; Fabbiani, F. P. A.; Parsons, S.; Sadler, P. J., Ruthenium(II) Arene Anticancer Complexes with Redox-Active Diamine Ligands. *Inorg. Chem.* **2009**, *48* (19), 9444-9453. DOI: 10.1021/ic9013366
68. Miller, J. S.; Min, K. S., Oxidation Leading to Reduction: Redox-Induced Electron Transfer (RIET). *Angew. Chem. Int. Ed.* **2009**, *48* (2), 262-272. DOI: 10.1002/anie.200705138
69. Piskunov, A. V.; Pashanova, K. I.; Bogomyakov, A. S.; Smolyaninov, I. V.; Starikov, A. G.; Fukin, G. K., Cobalt complexes with hemilabile *o*-iminobenzoquinonate ligands: a novel example of redox-induced electron transfer. *Dalton Trans.* **2018**, *47* (42), 15049-15060. DOI: 10.1039/c8dt02733a
70. Lohmeyer, L.; Schön, F.; Kaifer, E.; Himmel, H.-J., Stimulation of Redox-Induced Electron Transfer by Interligand Hydrogen Bonding in a Cobalt Complex with Redox-Active Guanidine Ligand. *Angew. Chem. Int. Ed.* **2021**, *60* (18), 10415-10422. DOI: 10.1002/anie.202101423
71. Talipov, M. R.; Boddada, A.; Lindeman, S. V.; Rathore, R., Does Koopmans’ Paradigm for 1-Electron Oxidation Always Hold? Breakdown of IP/ $E_{ox}$  Relationship for *p*-Hydroquinone Ethers and the Role of Methoxy Group Rotation. *J. Phys. Chem. Lett.* **2015**, *6* (17), 3373-3378. DOI: 10.1021/acs.jpcllett.5b01532

72. Elgrishi, N.; Kurtz, D. A.; Dempsey, J. L., Reaction Parameters Influencing Cobalt Hydride Formation Kinetics: Implications for Benchmarking H<sub>2</sub>-Evolution Catalysts. *J. Am. Chem. Soc.* **2017**, *139* (1), 239-244. DOI: 10.1021/jacs.6b10148
73. Kurtz, D. A.; Dhar, D.; Elgrishi, N.; Kandemir, B.; McWilliams, S. F.; Howland, W. C.; Chen, C.-H.; Dempsey, J. L., Redox-Induced Structural Reorganization Dictates Kinetics of Cobalt(III) Hydride Formation via Proton-Coupled Electron Transfer. *J. Am. Chem. Soc.* **2021**, *143* (9), 3393-3406. DOI: 10.1021/jacs.0c11992
74. Rieke, R. D.; Henry, W. P.; Arney, J. S., Two-Electron Reduction of ( $\eta^6$ -Naphthalene)tricarbonylchromium. Haptotropic Rearrangement to the ( $\eta^4$ -Naphthalene)tricarbonylchromium Dianion. *Inorg. Chem.* **1987**, *26* (3), 420-427. DOI: 10.1021/ic00250a016
75. Reingold, J. A.; Virkaitis, K. L.; Carpenter, G. B.; Sun, S.; Sweigart, D. A.; Czech, P. T.; Overly, K. R., Chemical and Electrochemical Reduction of Polyarene Manganese Tricarbonyl Cations: Hapticity Changes and Generation of *Syn*- and *Anti*-Facial Bimetallic  $\eta^4, \eta^6$ -Naphthalene Complexes. *J. Am. Chem. Soc.* **2005**, *127* (31), 11146-11158. DOI: 10.1021/ja0527370